Structures of actomyosin crossbridges in relaxed and rigor muscle fibers

Leepo C. Yu,* and Bernhard Brenner*‡
*National Institute of Arthritis and Muscoloskeletal and Skin Diseases, Laboratory of Physical Biology, National Institutes of Health, Bethesda, Maryland 20892; and ‡Institute of Physiology II, University of Tübingen, Tübingen, Federal Republic of Germany

ABSTRACT It was shown previously that a significant fraction of the myosin crossbridges is attached to actin in the skinned rabbit psoas fibers under relaxed conditions at low ionic strength and low temperature (Brenner, B., M. Schoenberg, J. M. Chalovich, L. E. Greene, and E. Eisenberg. 1982. *Proc. Natl. Acad. Sci. USA.* 79:7288–7291; Brenner, B., L. C. Lu, and R. J. Podolsky. 1984. *Biophys. J.* 46:299–306). In the present work, the structure of the attached crossbridges in the relaxed state between ionic strengths of 20 and 100 mM, as compared with that in the rigor state, is further examined by equatorial x-ray diffraction. Mass distributions projected along the fiber axis are reconstructed based on the first five equatorial reflections such that the spatial resolution is 128 Å.

The fraction of crossbridges attached under relaxed conditions are estimated to be in the range of 30% (at 100 mM ionic strength) and 60% (at 20 mM). The reconstructed density maps suggest that in the relaxed state, upon attachment the part of the crossbridge that centers around the thin filament is small, and the attachment does not significantly alter the center of mass of the myosin head distribution around the thick filament backbone. In contrast, accretion of mass in the rigor state occurs in a wider region surrounding the thin filament. In this case, mass in the surface region of the thick filament backbone is shifted slightly outward, probably by ~10 Å. A schematic model for interpreting the present data is presented.

INTRODUCTION

It was shown by mechanical measurements (Brenner et al., 1982) and equatorial x-ray diffraction studies (Brenner et al., 1984) that in a relaxed skinned rabbit psoas fiber, a substantial fraction of myosin heads (crossbridges) is attached to the thin filaments at low temperature (5°C) and low ionic strength (μ = 20 mM). Mechanical measurements revealed that the crossbridges under such conditions are in rapid equilibrium between attached and detached states. X-ray diffraction further showed that the number of attached crossbridges decreased as ionic strength increased. These properties exhibited by the crossbridges in a relaxed muscle correlated closely with those found for the weak-binding states of the actomyosin ATPase (Eisenberg and Hill, 1985). The existence of the weak-binding states of crossbridges in muscle lent strong support to the idea that during ATP hydrolysis, crossbridges, similar to actomyosin interaction in solution, alternate between weak-binding and strong-binding conformations. It was suggested that transition from the weak-binding to the strong-binding conformations results in force generation (Eisenberg and Hill, 1985). Because force generation is thought to result from a change in the structure of attached crossbridges, it is of particular interest to determine whether the structures of the attached weak binding states are different from those of the attached strong binding states.

Although the evidence for the existence of the weak binding crossbridge states in muscle is strong, detailed knowledge of the structure of such states is still lacking. Equatorial x-ray diffraction patterns (Brenner et al., 1984) showed that at low ionic strengths (e.g., μ = 20 mM), intensity of the [1, 1] reflection, I_{11}, was comparable with those of the rigor muscle. The intensity of the [1, 0] reflection, I_{10}, on the other hand, was greater than that in rigor state by a factor of 2. As it was pointed out in the previous study (Brenner et al., 1984), the difference in I_{10} could not simply be attributed to a difference in the number of crossbridges attached, since increasing the number of crossbridges in the relaxed configuration by lowering the ionic strength caused only small changes in I_{10} relative to that in I_{11}. It would be impossible to match the relaxed values in both I_{10} and I_{11} with the rigor values under the same set of conditions. Therefore, the large difference in I_{10} between the relaxed and the rigor states suggested a structural difference in the attached crossbridges. However, with only two reflections recorded, structural information is limited to ~280 Å resolution.

Results of electron microscopic studies of crosslinked myosin subfragment-1 (S1) to actin in the presence and in the absence of ATP also suggest structural differences in

Bernhard Brenner's present address is Abt. Allegemeine Physiologie, Universität Ulm, Ulm, Federal Republic of Germany.

0006-3495/89/03/441/13 $2.00

the attached S1 under those two conditions (Craig et al., 1985). However, the question remains whether the S1, unconstrained by lattice geometry but crosslinked to actin, represents the crossbridge in the muscle cells. In addition to the electron microscopic studies, two-dimensional x-ray diffraction studies show that the intensities of myosin-associated layer lines from a bundle of psoas fibers (Matsuda and Podolsky, 1984) and skinned frog sartorius muscle (Xu et al., 1987) were insensitive to the formation of attached crossbridges in the relaxed state, in contrast to the changes observed upon activation or rigor formation. This lack of sensitivity has not yet been fully explained. For the relaxed frog sartorius muscle, the lack of change in the diffraction patterns upon lowering the ionic strength mostly likely reflects a small increase in the number of attached crossbridges (up to ~15%) and an obvious ordering effect on the filament lattice. In the relaxed rabbit psoas fibers, under the low temperature conditions, myosin layer lines are weak at μ = 20 mM and 100 mM compared with those found at higher temperatures (Wray, 1987). Under the conditions used by Matsuda and Podolsky, the intensities of the myosin layer lines could be too low to provide definitive information on the effect of crossbridge attachment.

Here, five equatorial reflections, instead of two reflections previously used, were studied from single-skinned rabbit psoas fibers. With improved resolution, mass redistributions due to crossbridge attachment in the relaxed and the rigor state showed distinctly different patterns. In addition, normalization procedures were undertaken such that the attachment/detachment of crossbridges due to ordering/disordering effects of ionic strength was estimated quantitatively.

A brief account of this work has been reported earlier (Yu and Brenner, 1986).

METHODS

Fiber preparation

All experiments were performed on single, chemically skinned fibers of the rabbit *M. psoas major*, prepared according to Brenner (1983). Small bundles of fibers, ~1 mm in diameter, were isolated from the lateral margin of the *M. psoas major*. The bundles were held at their in situ length to the Sylgard (Dow Corning Corp., Midland, MI) covered bottom of a trough by stainless steel needles, and covered with chilled skinning solution (Brenner et al., 1984). For the first 30 min, 0.5% Triton X-100 was added to the skinning solution. Skinning solution was then renewed and for every 24 h thereafter. Fiber bundles were kept in skinning solution for up to 5 d at 4°C. No fibers older than 5 d were used because of occurrence of structural irregularities.

The usual method of preparing a single fiber is by peeling the fiber away from the bundle axis. In the process of peeling, parts of the fiber can easily be damaged by the connective tissue that forms a sheath surrounding the individual fiber. To avoid possible damage, a different technique was introduced (Brenner, 1983). The details are shown in Fig. 1 a 5–10-mm long section is cut from the stock bundle and pinned down at one end in chilled skinning solution. Fibers located near the original surface of the *M. psoas* are gripped by a pair of jeweller's forceps and moved out of the bundle by gently pulling along the fiber axis. To avoid stretching the fiber more than 10–15% of fiber length, several fibers are first removed from the bundle and discarded in order to loosen the initially compact fiber–connective tissue system. This method of isolation provides specimen free of connective tissue and without being overly stretched during dissection. Over stretch causes obvious disorder among the myofilaments as demonstrated by the greatly broadened peaks in the x-ray diffraction patterns.

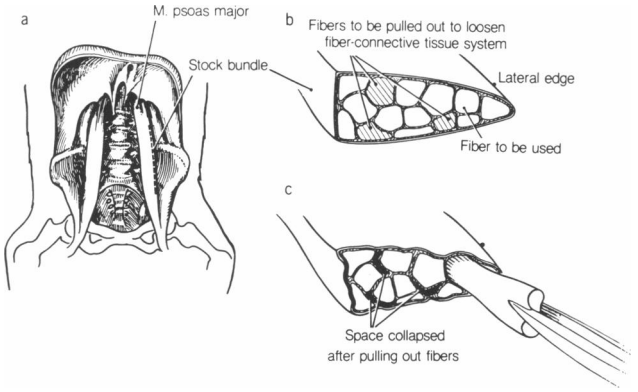

FIGURE 1 A technique for isolating single psoas fibers (Brenner, 1983). (*a*) Small bundles, ~1 mm in diameter and ~5 cm in length are isolated from the lateral edges of *M. psoas major*. (*b*) A section of the bundle, 5–10-mm long, is cut from the stock bundle and held down by a stainless steel pin in chilled skinning solution (Brenner et al., 1984). Fibers located near the original surface of the *M. psoas major* are gripped by a pair of jeweller's forceps and slid out of the bundle by gently pulling along the fiber axis. After pulling out several fibers, the fiber–connective tissue system is loosened. (*c*) The fiber to be used is isolated without being overstretched and is free of connective tissue.

The isolated fiber segments were mounted to the mechanical apparatus using a cyanoacrylate glue (Histoacryl, Braun Melsungen, FRG). Fiber length and cross-section were measured by light microscope (magnification 200).

Composition of solutions for the relaxed state was (in millimolars): 1 ATP, 1 EGTA, 3 $MgCl_2$, 10 immidazole, 1 dithiothreitol (DTT), pH 7.0; rigor solution, 2.5 EGTA, 2.5 EDTA, 10 immidazole, 1 DTT, pH 7.0. Ionic strength ranged between 20 and 100 mM. It was adjusted by adding various amounts of KPropionate, which maintained the lattice spacing constant between the ionic strengths used. KPropionate was found to maintain better lattice ordering than KCl, by producing sharper diffraction patterns. Temperature was 5°C. Sarcomere length was 2.3–2.4 μm.

X-ray experiments

Experimental setup for x-ray diffraction is shown in Fig. 2. The crucial factor in obtaining sharp and well defined equatorial diffraction patterns was to increase the signal to noise (S/N) ratio even at the expense of count rate. To achieve high S/N ratio, an important element

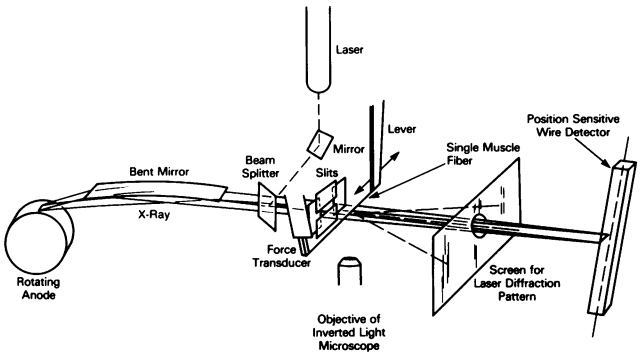

FIGURE 2 Schematic diagram of experimental setup. X-ray source was a rotating anode (1) (Elliott GX-6, Marconi Avionics, Hertfordshire, England) in the line focus configuration and was foreshortened at a take-off angle of 4°. The x-ray beam was focused by a 200-mm gold-coated polished quartz mirror (2) (Astron, Middlesex, England) with a beam defining slit in the middle of the bender (3). The parasitic scatter from slit 3 was eliminated by slit 4 placed immediately in front of the chamber holding the fiber (9), which was 20 cm downstream from the center of the mirror. The slits (designed and constructed by C. Crist, National Institutes of Health) were adjustable by movements of 5 μm. Sarcomere length was determined by a helium neon laser (7). The laser beam was directed through the slits (4) by a beam splitter (8) (Melles Griot, Irvine, CA), such that the laser beam followed the same path as that of the x-ray after the slits. As a result, locating the fiber (9), which was held by two adjustable carbon fiber tips (10 and 11), was greatly facilitated. Homogeneity of the sarcomere distribution was monitored by an inverted light microscope (12), placed beneath the bottom of the fiber chamber. Specimen to detector distance was 33 cm. The beam stop (5), a strip of nickel 250-μm thick and 0.7-mm wide, was placed 22 cm from the fiber. Data were recorded by an electronic position sensitive detector (6). The x-ray path was flushed with helium except where the fiber chamber was placed.

in the camera design for the small sized specimen was the proper arrangement of the slits, slit 3 at the center of the mirror bender and slit 4 in front of the specimen holder, ~20-cm downstream. The slit 4, constructed by Charles Crist (National Institutes of Health), was adjustable to within 5 μm. The beam was first defined by slit 3, such that the beam size at the specimen was comparable with the size of the fiber. Scatter from slit 3 was eliminated by slit 4. The beamstop was situated 22 cm from the specimen, such that the splash from the beamstop was relatively low at the position of the [1, 0] reflection. The entire beam path was flushed with helium.

Diffraction patterns were recorded digitally by a position sensitive detector constructed by Lippo Yu, with a spatial resolution of ~90 μm. Linearity of the detector was checked to be within 1% for the length used in recording patterns (~15 mm). Exposure time generally was 5,000 s in order to obtain sufficient statistics for reflections at least up to [3, 1]. Occasionally, a fiber was exposed for 8–12 h. With such long exposure, reflections up to [5, 0] could be resolved above noise level of patterns of relaxed fibers at μ = 20 mM.

The diffraction patterns of the fibers after several exposures were reversible, although at the end of the experiments (after ~8 h) they usually showed signs of deterioration with the widths of the reflections becoming wider and the higher order reflections, weaker. Generally, 2–4 different solutions were applied to each fiber. The order of applied solutions was random, but frequently rigor patterns were obtained last.

Data analysis

Integrated intensities of each reflection were subsequently obtained by a nonlinear least squares fit algorithm (Knott, 1979) applied to the experimental data as described previously for an intact whole frog sartorius muscle (Yu et al., 1985). However, it was found that modifications were necessary for the present study because we used different preparations (single fiber versus whole muscle) and different experimental conditions (laboratory x-ray source versus synchrotron radiation). The background function applied in the present study was of the form

$$A \cdot \exp(Bx) + C \cdot \exp(Dx) + E. \quad (1)$$

The function used to fit each reflection peak was of Lorentzian form:

$$L(x) = A/[1 + (x - x_0)^2/\sigma^2], \quad (2)$$

where A is the amplitude; x_0, center of the peak; 2σ is the full width at half maximum (FWHM) of the peak. Gaussian functions did not fit the present x-ray diagrams as well as Lorentzian functions.

Fourier synthesis

Averaged intensity data were used to perform Fourier synthesis for obtaining two-dimensional axially projected density maps in a hexagonal lattice. At relatively low resolution, we assumed that the myofilaments were centrosymmetric. The phases for [1, 0] and [1 ,1] were shown to be $(++)$[1] in order to show positive masses at the filament sites (Huxley, 1968). Other phases were selected according to criteria similar to those used previously (Yu et al., 1985) and further aided by modeling (Yu, 1989 [accompanying paper]). Although we have examined all reflections up to [3, 1], emphasis was placed on the first five reflections, up to [3, 0], since we optimized parameters of the modeling to match the five reflections.

Phases which gave rise to cases showing thick or thin filaments with low density cores were rejected because it was shown by modeling (Yu et al., 1985) and further supported by more recent work (Yu, unpublished data) that such low density features produced at present resolution would require hollow cores ~50 Å in diameter that run the entire length of the filaments. In the absence of evidence for such filament structures, these cases were rejected. An additional constraint was that ratio of the masses, above the minimum density level of the unit cell, of the myosin filament backbone to the thin filament should be less or equal to the same ratio calculated from biochemical data with no crossbridges attached to the thin filament. Since there is ample evidence that there are crossbridges attached under the conditions studied here (Brenner et al., 1982, 1984), the actual mass ratio should be lower than the theoretical ratio of 2.6 (Yu et al., 1985). Thus the theoretical ratio served as an upper limit.

Using the criterion that peak densities were at the centers of the filaments, phase of [3, 0] was required to be (+) (Yu, 1989). The phase combination $(+++++)$[2] was rejected because of the density at the thin filament is very low, but overly dominant at the thick filament. Therefore, only three other possible combinations remained: (*i*) $(++-++)$, (*ii*) $(++--+)$, and (*iii*) $(+++-+)$.

The mass of attached crossbridges spanning across the interfilament space should bring the density level between the thick filament backbone

[1]A "+" phase is equal to 0°; a "−" phase is 180°.

[2]The phases are listed in the same order as the reflections, i.e., [1, 0], [1, 1], [2, 0], [2, 1], and [3, 0].

and the thin filament higher than the minimum level of the entire unit cell. This constraint excluded phase set *iii*. The choice between *i* and *ii* was more difficult. Phase set *ii* showed a low, although not the lowest, density level between the backbone and the thin filaments. Again this reduced the likelihood of phase set *ii*, although it could not be rejected unambiguously. In phase set *i*, the said density level is about one-third that of the thick filament backbone, which is consistent with myosin heads in axial projection. The center of the annular mass is located at ~13 nm. This is consistent with the estimated radial position of myosin heads (12–13 nm) in intact relaxed frog muscle at the same lattice spacing (Haselgrove, 1980). Therefore, the phase set (++−++) is more likely to be the correct one. However, in the following discussions, it will be shown that mass redistribution between relaxed and rigor conditions is not sensitive as to which phase combination among *i* and *ii* is chosen, provided that the phases remain unchanged in transition from the relaxed to the rigor state.

Amplitudes from diffracting plane of the same spacing were set to be equal, since using the present approach, one could not distinguish contributions from various crystallographic planes with equal spacings. It was further assumed that $F_{12} = F_{21}$ for the fourth order [2, 1], and $F_{13} = F_{31}$ for the 7th order [3, 1], as required by six-fold symmetry.

Normalization

The entire diffraction pattern was first normalized by the direct x-ray beam transmitted through the semi-transparent beamstop (Ni, 250-μm thick). Care was taken that the same part of the fiber was exposed to x-ray while bathed in various solutions. Since the lattice volume was kept constant, the mass exposed to the x-ray beam remained constant. Thus the zeroth order term, F_{oo}, was set to be 2,000 in arbitrary units for all the patterns. Before each high resolution pattern (p) was recorded, a relaxed pattern at μ = 20 mM was first obtained only for a short exposure (500 s), to establish sufficient statistics for the intensity of the [1, 0] reflection (I_{10}). Amplitudes of all reflections in pattern (p) that followed were normalized with respect to this I_{10}. The amplitude of the [1, 0] reflection of the μ = 20 mM pattern was set to be 100. Thus all other amplitudes obtained under various conditions were normalized uniformly.

Density maps and difference maps

Calculations and display of two-dimensional density maps were carried out on a VAX computer (Digital Equipment Corp., Marlboro, MA) using the image processing system PIC (Trus and Steven, 1981). The hexagonal lattice was represented on a square lattice, with each pixel sampling 10 Å (Yu et al., 1985; Yu, 1989). Density distribution was represented by a grey scale where the lightest tone represents highest density.

Diameter of filaments (apparent diameter) in the density maps is defined as the full width at half maximum relative to the lowest density level in the unit cell. At low resolution, objects are smeared so that they appear larger than their actual sizes. Based on five reflections, the diameter of the thick filament backbone appears to be ~180 Å (Yu et al., 1985) even though the actual diameter is probably ~160 Å. Similarly, a thin filament is enlarged to 150 Å in apparent diameter (Yu et al., 1985), while the actual diameter is ~100 Å (Egelman and Padron, 1984).

Upon changing of conditions, redistribution of mass occurred. The difference in density, or equivalently, the difference in mass distribution in the two-dimensional maps obtained by Fourier syntheses represented net transfer of mass projected onto the equatorial plane. To visualize net redistribution of mass, color-coded difference maps were constructed to distinguish regions with net loss from net gain and no effective change. Color maps were displayed on a DEANSA system and color photos were taken directly from a Matrix system.

RESULTS

Fig. 3 shows equatorial diffraction patterns from single skinned psoas fibers in the (*a*) relaxed state at μ = 20 mM, (*c*) relaxed state at μ = 100 mM, and (*d*) rigor state at μ = 100 mM. Pattern 3 *a* was taken over 12 h whereby 12 reflections (up to [5, 0]) could be resolved above background. For normal exposures (5,000 s) reflections up to [3, 1] are clearly resolved.

Equatorial intensities

Under all conditions studied, the first two reflections [1, 0] and [1, 1] were ~10-fold stronger than those beyond [1, 1] (Table 1). However, the higher order reflections up to [3, 2] remained clearly resolved above background. Although all the patterns showed well defined peaks, the sharpness of the reflections in the patterns was improved as ionic strength was lowered, indicating that lowering ionic strength had an ordering effect on the lattice. In fact, for 8–12 h of exposure, reflections up to [4,2] could frequently be resolved in the relaxed state at μ = 20, 50 mM but at $\mu \geq$ 100 mM, higher orders beyond [3, 2] were seldom observed. Rigor state was less affected by ionic strength, but generally only nine reflections (up to [3, 2]) were observable at $\mu \geq$ 100 mM.

The equatorial patterns were fitted almost exactly by the Lorentzian functions with two exponential functions as the background as shown by the goodness of the fit in Fig. 3. The widths of reflection peaks σ_{hk}, deconvoluted from the width of the x-ray beam, increased linearly with reflection angle. The data could not be fitted with σ_{hk} varying quadratically with reflection angle. This suggests that the broadening fo peaks mainly resulted from the distribution of interfilament spacing, d_{10} (~1–3%) (see Appendix, Yu et al., 1985), rather than liquid-like disorder (disorder of the second kind) of the filament lattice.

The lattice spacing d_{10} remained the same at 385 Å for all the conditons studied in the present work.

The first five phases most likely remain unchanged under the conditions studied

One striking feature of the present results is that while [1, 0] and [1, 1] intensities changed considerably with various conditions, the higher order reflections, [2, 0], [2, 1], [3, 0], remained almost identical. For the relaxed state, the results were obtained at several graded levels of

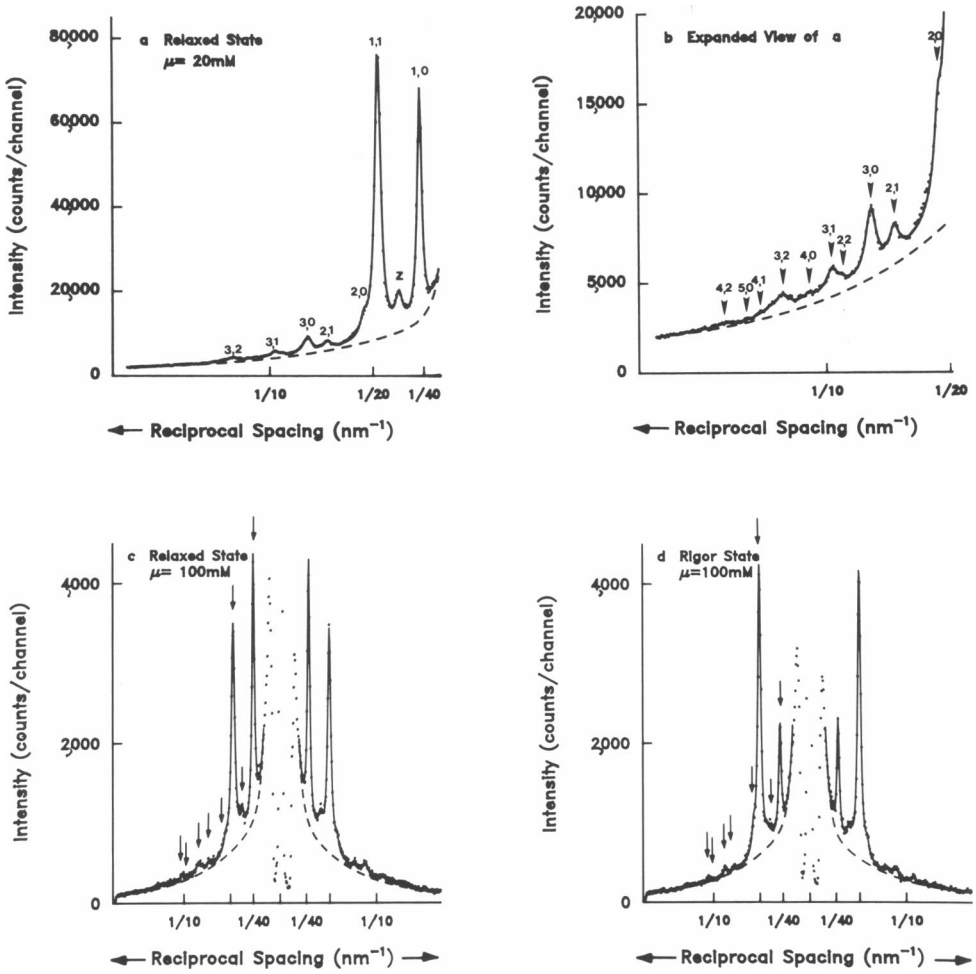

FIGURE 3 Equatorial diffraction patterns from single skinned psoas fibers in the (*a*) relaxed state at μ = 20 mM, (*c*) relaxed state at μ = 100 mM, and (*d*) rigor state at μ = 100 mM. *b* is the same as a except that intensity is plotted on a different scale. Dots are the original data; (*solid lines*) are the fitted curves with exponential functions used for the background (*dotted lines*) and Lorentzian functions for the reflection peaks (see text, Eqs. 1 and 2). Reflections indexed according to the hexagonal lattice and reflection from the Z-line are labeled as shown. Exposure time for *a* was 12 h; for *c* and *d*, 5000 s. Data shown in Table 1 were mostly collected in 5,000 s. Sarcomere length, 2.3 μm. Temperature, 5°C.

TABLE 1 Intensities of individual equatorial reflections

	I_{10}	I_{11}	I_{20}	I_{21}	I_{30}	I_{22}	I_{31}
Relaxed							
μ = 20 mM (n^* = 25)	1	1.83 ± 0.006‡	0.11 ± 0.006	0.03 ± 0.002	0.14 ± 0.006	0.01 ± 0.002	0.06 ± 0.004
μ 50 mM (n = 13)	1.01 ± 0.01	1.57 ± 0.09	0.10 ± 0.006	0.04 ± 0.003	0.11 ± 0.008	0.005 ± 0.002	0.05 ± 0.006
μ = 80 mM (n = 18)	1.08 ± 0.017	1.26 ± 0.08	0.10 ± 0.007	0.05 ± 0.002	0.10 ± 0.007	0.014 ± 0.005	0.04 ± 0.005
μ = 100 mM (n = 16)	1.19 ± 0.015	1.23 ± 0.05	0.09 ± 0.005	0.04 ± 0.002	0.10 ± 0.005	0.01 ± 0.002	0.04 ± 0.005
Rigor							
μ = 100 mM (n = 16)	0.56 ± 0.021	2.14 ± 0.14	0.10 ± 0.01	0.04 ± 0.005	0.09 ± 0.008	0.02 ± 0.005	0.05 ± 0.05

*n, number of data points used; each data point is from one side of a diffraction pattern.
‡SEM.

ionic strength. If there were phase changes, it would imply that with a change of 20–30 mM in ionic strength, the amplitudes would cross the zero level and reach similar magnitude but different phases. Such a case is highly improbable. As for the rigor state, the phases may not remain the same. However, the amplitudes of the higher orders are very similar between the relaxed and the rigor states. It would be rather coincidental, although not impossible, that after a phase change, the amplitudes remain approximately the same. Therefore, we consider phase changes in the first five phases in the relaxed and the rigor states as unlikely.

Density maps

Fig. 4 shows the two dimensional electron density maps reconstructed according to the phase set *i* (++−++) (Fig. 4 *a*) for the relaxed state and (Fig. 4 *b*) the rigor state at μ = 100 mM. Fig. 4 shows that the pronounced feature in the density maps is that the thick filament is resolved into a backbone structure with an annular shell of mass of lower density surrounding it, which is most likely that of the myosin heads, although myosin heads need not be restricted only to this region. The radius of the annular mass is ~13 nm. The relative amounts of mass in each region depend on the physiological states. Another feature is that the apparent diameter of thin filament appears to be larger in the rigor state.

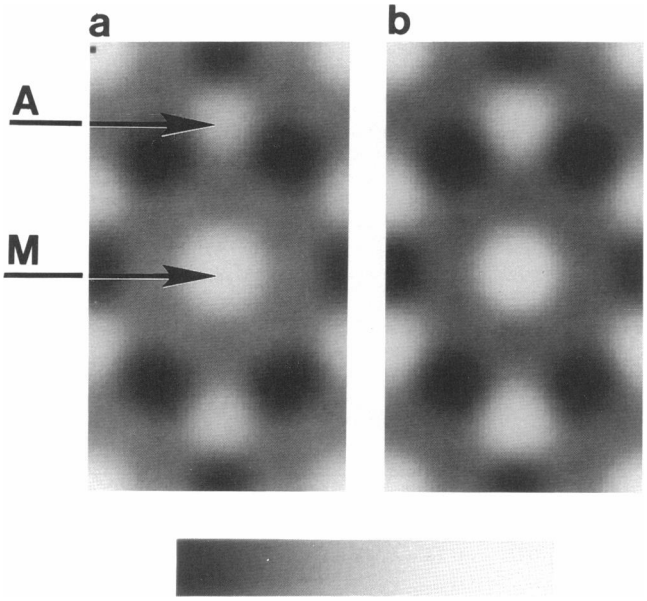

FIGURE 4 Two-dimensional electron density maps of the filament lattice in axial projection obtained by inverse Fourier transform of experimental amplitudes up to [3, 0]. Phase set (++−++) for the five reflections [1, 0], [1, 1], [2, 0], [2, 1], and [3, 0] was used. μ = 100 mM. (*a*) The relaxed state; (*b*) the rigor state. Two unit cells are arranged on a square lattice, with each pixel sampling 1 nm. The highest density is shown by the lightest tone on the grey scale. The perpendicular distance between two thick filaments (d_{10}) is 38 nm. *A*, thin filament; *M*, thick filament.

The background density level does not remain constant among the relaxed states at various ionic strengths. Since the amount of mass exposed to x-ray was uniformly normalized, a change in the minimum density level of the unit cell indicates that the amount of mass assembled in the ordered structure has changed. Total ordered mass decreased by ~8% as ionic strength was raised from μ = 20 to 100 mM in the relaxed muscle (Table 2). Because the decrease in ordered mass is accompanied by broadening of peaks and weakening of higher order reflections particularly beyond [3, 1], we conclude that the myofilament lattice in the relaxed state is not as well ordered as ionic strength is increased. Some of the protein mass has become background mass, increasing the diffuse scattering in the x-ray diagram (Poulsen and Lowy, 1983). The minimum density level in the rigor state is generally somewhat lower than the relaxed state at the corresponding ionic strength, but the amount of difference is smaller, ~3%.

Difference maps

One of the major goals of the present study is to determine differences in crossbridge structure under various conditions. Color-coded difference density maps provided a sensitive overall view of net mass shift upon changing of

TABLE 2 Calculations of mass distributions*

Condition	Minimum density level	Total visible mass‡	Mass associated with thick filament backbone§	Mass associated with one thin filament‖
mM				
Relaxed				
μ = 20	0.2853	1,046	311	149
50	0.2960	1,010	308	145
80	0.3074	972	306	137
100	0.3104	962	307	136
Rigor				
100	0.2990	1,000	297	160

*The zeroth order term F_{oo} is assumed to be 2,000 in arbitrary units for all conditions. Phase set used: (++−−+).

‡Total visible mass is the sum of all densities in the unit cell above the minimum level (Yu et al., 1985).

§Total mass integrated over circular areas 200 Å in diameter with the center at the lattice point of the backbone. Mass under all conditions was calculated above the same density level (0.2853), which is the minimum level for the relaxed state at μ = 20 mM.

‖Total mass integrated over circular areas 150 Å in diameter with the center at the trigonal point. Method of normalization is the same as in footnote §.

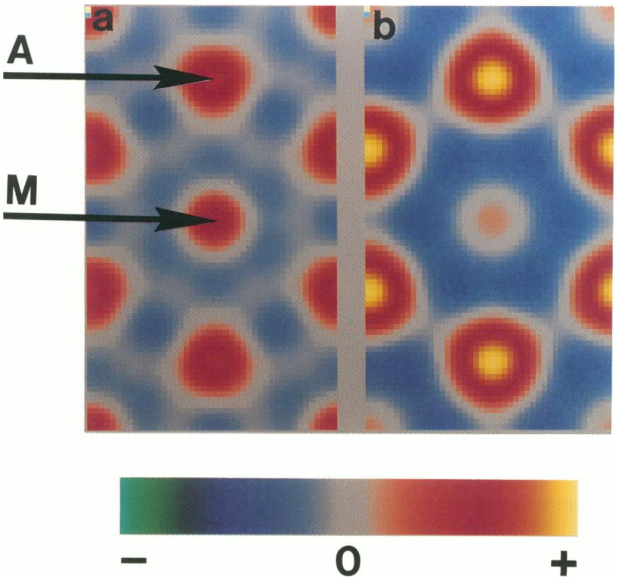

FIGURE 5 Color-coded difference maps showing difference in mass distributions in the unit cells upon changing of conditions. Phases are assumed to remain unchanged at (++−++). In *a*, densities of the relaxed state at μ = 100 mM are subtracted from those of the relaxed state at μ = 20 mM (rel→rel); (*b*) densities of the relaxed state at μ = 100 mM are subtracted from those of the rigor state at the same μ (rel→rigor). Gray color represents insiginficiant change (±5%). Increasing gain of mass is shown with red to yellow; increasing loss, blue to green.

conditions. Transition between the two relaxed states (rel→rel) (Fig. 5 *a*) exhibits mass redistribution characteristically different from that between the relaxed and the rigor states (rel→rigor) (Fig. 5 *b*). In Fig. 5 *a*, the amount of increase of mass at the thin filament site is 9% of the total thin filament mass and occurs in a region 140 Å in diameter. For the (rel→rigor) cases (Fig. 5 *b*), the mass increase is 17% and occurs in a larger region, 180 Å in diameter.

In the relaxed state as ionic strength is lowered, there is a gain of mass at the center of the thick filament. However, the overall net change is very small (~1%) within the apparent diameter 200 Å of the backbone. If one calculates the net mass change within a diameter of 220 Å there is even less loss. A reasonable explanation is that the backbone is better ordered at the lattice points or the backbone is slightly tighter packed as ionic strength is lowered. Models similar to those described in Yu (1989) suggest that the gain at the center of the thick filament probably reflects a slightly smaller diameter (by ~5 Å). In the case of rel→rigor, on the other hand, the backbone shows a net loss of ~4% within an area of 200 Å in diameter. The loss is greater if integration of density is taken over a larger area: the loss apparently extends outward beginning at ~70 Å from the center of the filament (Fig. 6). At the present resolution, it is difficult to draw a boundary between the backbone structure and the annular shell of mass of the myosin heads. Because the mass shift begins at ~70 Å from the filament center, it is likely that mass which was originally on the surface region of the backbone has shifted outward.

Differences in mass redistributions are insensitive to selection of phase set *i* or *ii*

Fig. 7 *a* shows the density map by using the phase combination (++−−+) (set *ii*) instead of (++−++) for the relaxed state. The rigor density map has similar characteristics. The density level between the thick and the thin filaments is low, ~20% of the peak density at the center of the thick filament. According to model calculations (Yu, 1989), the center of the myosin head distribution is approximately located 10–12 nm from the center of the backbone. This phase set reflects a more compact packing of S1 than phase set (++−++). However, the difference maps (rel→rel, Fig. 7 *b*; and rel→rigor, Fig. 7 *c*) are almost identical to Fig. 5 *a* and *b*. In other words, the three main characteristics of the difference maps, i.e., the difference in accretions of mass around the thin filaments between (rel→rel) and (rel→rigor), the changes in background density levels in the rel→rel

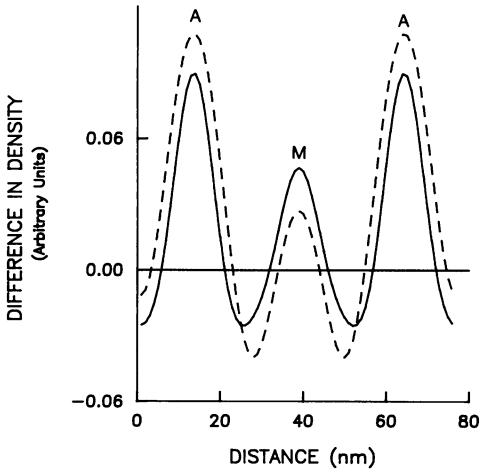

FIGURE 6 Density profiles of the difference maps shown in Fig. 5 along the vertical lines joining the centers of the thin and the thick filaments. *M*, center of the thick filament; *A*, center of the thin filament. *Solid line*, density redistribution between the two relaxed states (rel→rel) at μ = 100 mM and 20 mM (Fig. 5 *a*); *dashed line*, redistribution between relaxed and rigor states (rel→rigor) at μ = 100 mM. Maximum of the vertical scale (0.12) represents ~15% of the maximum densities in Fig. 4.

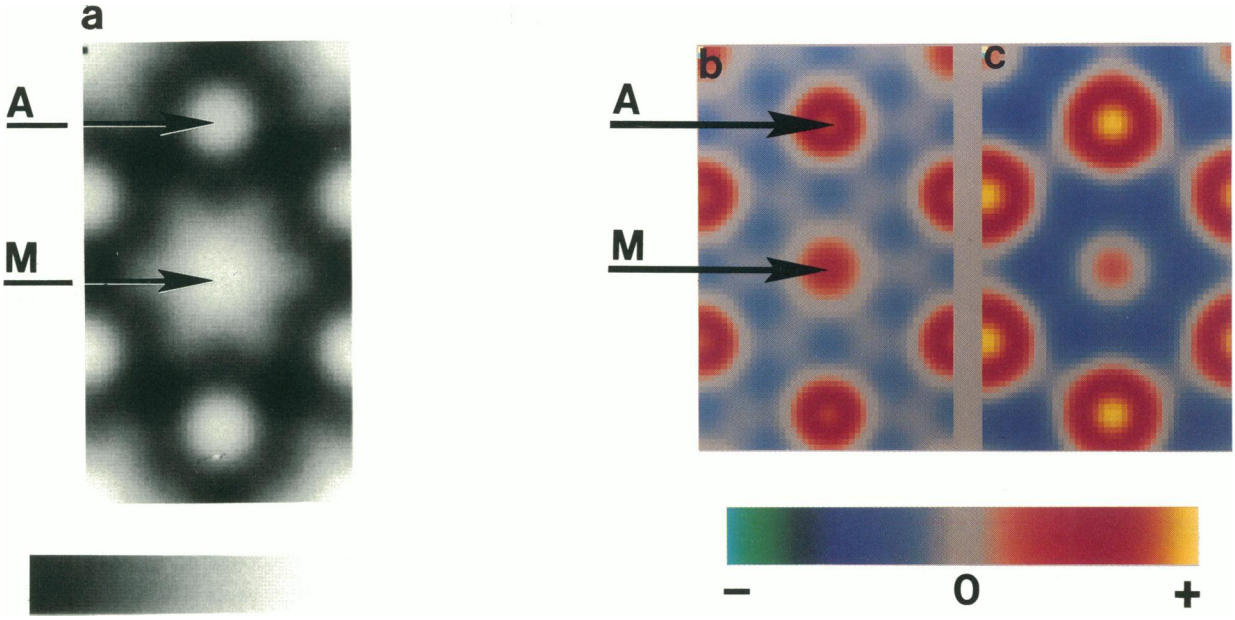

FIGURE 7 (*a*) Electron density maps of the filament lattice of the relaxed state at μ = 100 mM reconstructed from the same experimental amplitudes as in Fig. 4 *a* but with phase set (+ + − − +). (*b*) Difference maps between relaxed states at μ = 100 mM and 20 mM (rel→rel); (*c*) between relaxed and rigor states at μ = 100 mM (rel→rigor).

cases, and the outward mass shift in the rel→rigor transition, are independent of which of these two phase sets is chosen, as long as the first five phases remain unchanged upon changing the conditions.

Sensitivity of the features of the difference maps to series termination and uncertainties in amplitudes

To determine whether the features in the difference maps were direct consequence of series termination (Yu, 1989), temperature factors (Fraser and MacRae, 1973) of the form exp $(-B/4d^2)$ were applied to the measured intensities where B ranged between 4.5×10^3 and 1.5×10^5 and d was the lattice spacing of Bragg planes. It was found that the difference maps maintain several main characteristics: the areas of mass increase surrounding the thin filament still assume different sizes between rel→rig conditions; there is still a slight mass gain at the center of the thick filament in the case of rel→rel; and part of the mass of the backbone appears to move outward in transition from the relaxed to the rigor state. On the other hand, loss of mass in the case of rel→rel becomes uniform throughout the interfilament space.

The features observed in the difference maps are not significantly affected if each amplitude is added or subtracted by its standard errors of the mean. However, in some instances, the six-fold symmetry of mass loss in the rel→rel case is transformed to uniform loss surrounding the thick filament.

Effects of including [2, 2] and [3, 1]

With two additional reflections, the spatial resolution of the reconstructed density maps is improved to 107 Å, but an additional fourfold of phase combinations are possible. We did examine all 32 combinations with phases for [1, 0] and [1, 1] set to (+ +). Those density maps that were rejected based on the selection criteria for the first five reflections still remained unsatisfactory despite the addition of two more reflections. However, at the present time we are unable to determine which combination is the correct one among the eight possible combinations (adding [2, 2] and [3, 1] to phase sets *i* and *ii*). [2, 2] is a very weak reflection, particularly in the relaxed state, with high uncertainties in all the cases studied. The assignment of either (+) or (−) phase does not alter the appearance of the density maps significantly. However, models that produce intensities close to the experimental amplitudes and the phase set (+ + − + +) generally show that [2, 2] assumes (+) phases for the relaxed state, while (−) for the rigor state. For [3, 1], the phase is more likely to be

(−). Otherwise, the size of the thick filament appears to be too small (~130 Å). However, regardless whether (+−) or (−−) is chosen for [2, 2] and [3, 1], the main conclusion remains the same that the increase of mass around the thin filament is limited to a smaller area in the relaxed state; in transition to rigor, some mass that is originally a part of the backbone is shifted outward; and the lattice is better ordered at low ionic strength in the relaxed state.

DISCUSSION

The present study represents more than twofold improvement in spatial resolution over the previous work (Brenner et al., 1984). The lattice spacing is constant and each reflection is normalized with respect to one reflection, i.e., I_{10} under relaxing condition at μ = 20 mM. Thus, direct comparison of mass distributions in the unit cell under various conditions is possible.

In the relaxed muscle at 20 mM $\leq \mu \leq$ 100 mM, the total amount of mass associated with the thin filaments is higher than what would be expected if there were no crossbridges attached to them. The theoretical mass ratio of thick filament backbone to a bare thin filament is as high as 2.6 (Squire, 1981; Yu et al., 1985), but in the present study, the highest ratio which is found at μ = 100 mM is 2.3 (Table 2), indicating that there is extra mass added to the thin filament. If we make the simplifying assumption that in axial projection the attachment configurations are comparable for the relaxed and rigor states, and that the fraction of crossbridges attached in the rigor state is taken as 100%, the fraction of crossbridges attached in the relaxed state is calculated to be 60% at μ = 20 mM and 33% at μ = 100 mM (Table 3). By measuring the rapid stiffness of single skinned psoas fibers, Brenner et al. (1982) found that the fraction of crossbridges attached in the relaxed state at μ = 20 mM and 5°C was at least 50% of the rigor value. This estimate is also in good agreement with our previous finding (~65–90%), based on the effective actin concentration in the skinned psoas fiber being 1.5–6.5 mM (Brenner et al., 1986*a*; Brenner, et al., 1986*b*). Conclusions based on attachment and detachment rate constants gave similar fraction of crossbridges attached to actin at μ = 20 mM (Schoenberg, 1988). However, the present estimate is likely an underestimate, since it is possible that in axial projection the "relaxed" crossbridges are attached in a more perpendicular orientation than the rigor crossbridges and thus resulting in lower density projected onto the thin filament.

TABLE 3 Amount of mass increase* immediately surrounding the thin filament relative to the rigor state‡

Condition	Mass increase
mM	%
Rigor	
μ = 100	100
Relaxed	
μ = 20	61
50	54
80	38
100	33

*Mass increase is defined as the amount of mass in excess of the thin filament mass.

‡Mass associated with the thin filament relative to the backbone of the thick filament (A/M_o) in the area of 150 Å in diameter (Table 2, column 5) is assumed to be of the form $(A_o + \Delta M)/M_o$, where A_o is the mass of a bare thin filament, M_o is the mass of the backbone of the thick filament (Table 2, column 4), ΔM is the mass increase due to attachment of the crossbridges. According to experimental evidence as collected in the book by Squire (1981), A_o/M_o = 0.39, and hence ΔM is derived based on the above expression. All ΔM in the relaxed states are normalized with respect to ΔM in the rigor state, assuming that the attachment orientation in those two states are the same.

Significant features of the difference maps

The present study finds that the extra mass added on to the thin filament due to crossbridge attachment in the relaxed state does nto significantly alter the apparent diameter of the thin filament. That is, the spatial extent of the changes occurs within areas that are below the resolution of the present work. The apparent diameter, which is defined as the full width at half maximum density, of the thin filament is ~150 Å regardless whether the actual diameter is 75 or 115 Å (Yu et al., 1985). If the actual diameter of the thin filament is 100 Å (Egleman and Padron, 1984), then the width of the annular area of accretion of mass in axial projection could be ~15 Å. The rigor state, on the other hand, induces more mass transfer and enlarges the thin filament to appear ~180 Å in apparent diameter, which suggests that the width of annular area of accretion of mass could be ~50 Å. It should be emphasized that this characteristic mass redistribution is independent of the choice of phase set (++−++) or (++−−+). Furthermore, model calculations suggest that the change or the lack of it in the apparent diameter is not simply the result of different amounts of mass increase at the trigonal point, the location of thin filament. That is, a difference simply in the number of crossbridges attached to the thin filament cannot account for the difference observed for crossbridge attached under relaxing and rigor conditions.

Interpretation of the results

Fig. 8 illustrates one possible interpretation of the experimental data. The head portion of the myosin molecule is ~190-Å long and 50-Å wide (Winkelman et al., 1985). The surface to surface distance between the thick filament backbone and the thin filament is ~130 Å. The myosin heads must be either oriented with their long axis at an acute angle to the thick filament axis and/or slewed around the backbone, as suggested by images reconstructed from isolated thick filaments of frog (Stewart and Kensler, 1986). Under relaxing conditions, the crossbridges probably undergo fluctuations around their equilibrium positions. Therefore, the end-on view of the myosin heads at present resolution appears as an halo of mass surrounding the thick filament backbone. By virtue of its large size relative to the intersurface spacing, the myosin heads can reach the thin filament readily by small additional tilting and/or by small azimuthal movements. Fig. 8 *a* describes the case where few of the crossbridges are attached at any moment. Here the crossbridges undergo fluctuations such that only small fraction of time is spent in the vicinity of the thin filaments. As the actomyosin affinity increases upon lowering the ionic strength (Fig. 8 *b*), the fraction of time the myosin heads associated with the thin filament increases, but the extent of fluctuations needs only to be slightly affected. The fact that upon lowering ionic strength, the change in I_{10} is small compared with the change in I_{11} suggests that in axial projection the distribution of myosin heads surrounding the thick filament backbone is not disturbed substantially. The small change in I_{10} suggests that the attachment of crossbridges in the relaxed state (weak binding crossbridges) does not involve significant radial movement of the mass of myosin head but only a small domain of the myosin head may become concentrated around the thin filament. In Fig. 8 *c* crossbridges formed in the rigor state have the tail part of the myosin head or S2 moved away slightly from the backbone. Either by a slewing motion around the thin filament and/or axially tilting closer to the thin filament, a large domain of the myosin head can be brought to concentrate around the thin filament, thereby causing a larger axially projected cross-section. The exact orientation of attachment cannot be determined from equatorial projections and at the present resolution interpretation can only be qualitative. But the present data do place a rather restrictive constraint on possible models describing the actomyosin crossbridge formation.

Two-dimensional x-ray diffraction study on the rabbit psoas muscle (Matsuda and Podolsky, 1984) showed that the myosin related layer lines are insensitive to crossbridge attachment in the relaxed state. Although the ordering effects of lowering the ionic strength on the layer lines have not yet been investigated, the present model appears to be consistent with the two-dimensional results. Since little disturbance is proposed for the myosin head distribution in axial projection upon attachment in the relaxed state, the helical order of the myosin heads might also be preserved, causing little change in the layer lines.

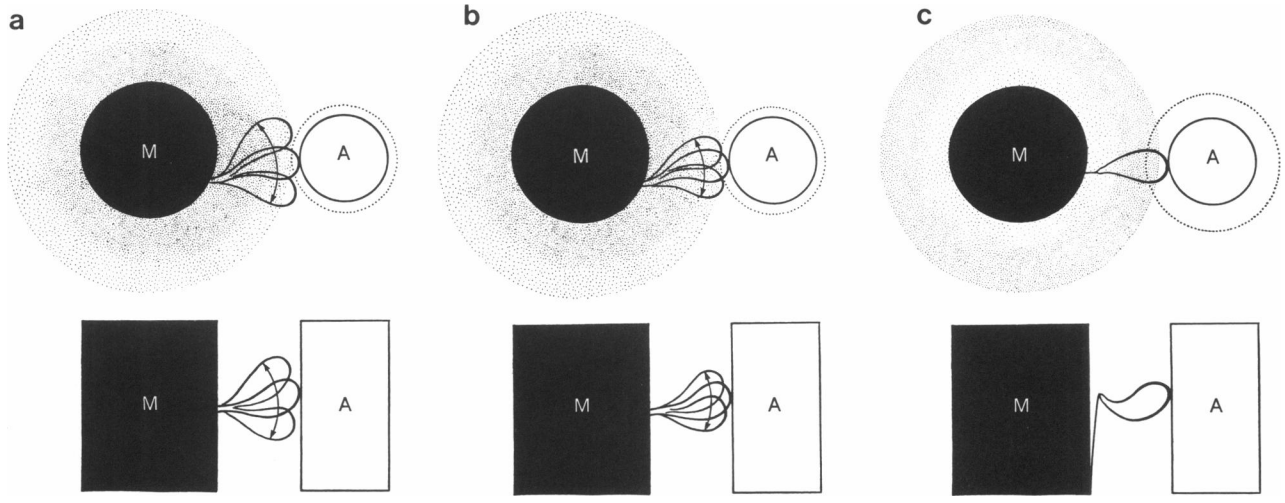

FIGURE 8 A schematic representation of an interpretation of the experimental results. *M*, thick filament backbone; *A*, thin filament. The distribution of myosin heads is represented as a halo surrounding the backbone. (*a*) A situation where few myosin heads are attached to the thin filament at any moment. The myosin heads undergo fluctuations around their equilibrium positions. (*b*) As the actomyosin affinity increases, the myosin heads spend increasing amounts of time in the region of the thin filament, but the fluctuations continue. The part of myosin mass centered around the thin filament helix is small. (*c*) In the rigor state, mass close to the backbone surface moves slightly outward and closer to the thin filament either by an axial tilt or by slewing.

The current model is also consistent with a crossbridge attachment model suggested by Goody and Holmes (1983), where transition from one site binding on the thin filament to two-site binding brings a change in the angle of attachment. One site binding could allow flexibility in the crossbridges and could involve only a small domain of the myosin head. The second site binding in rigor may involve a larger domain of the myosin head, thus shifting mass away from the thick filament area toward the thin filament. A similar model has been proposed by Podolsky and Arata (1988). Thus such ideas are well consistent with the model proposed in Fig. 8.

It should be mentioned that in transition to rigor state, if the center of the entire population of crossbridges is shifted outward, the movement is limited to ~10 Å to account for the small changes observed in the higher orders (see Table 1, Yu, 1989). However, if only parts of the myosin are involved, the radial distance shifted could be greater.

Relation to muscle contraction

In the present study we have demonstrated that the weak binding crossbridges attached in a relaxed muscle have different configuration from attached strong binding crossbridges in rigor muscle. The significance of the weak-binding crossbridges in muscle has been a subject of recent debate. To account for the time course of force and x-ray diffraction patterns during the rising phase of a tetanus Huxley and Kress (1985) proposed that the transition into force-generating states is a two-step process, in which crossbridges first enter an attached "pre–force-generating state" and through a subsequent transition, enter into the "force-generating state." Different from the actin affinity of the weak-binding crossbridges described in the present study which increases about fivefold with Ca^{++} (Wagner and Giniger, 1981), the attachment of the pre-force generating crossbridges proposed by Huxley-Kress is assumed to be blocked or unblocked by tropomyosin depending on the presence of Ca^{++}. So far, kinetic and structural properties of such postulated crossbridges have not yet been characterized. On the other hand, according to the crossbridge theory proposed by Eisenberg and Hill (1985), force is generated by the attached crossbridges following a transition from the weak- to the strong-binding states, where both the weak-binding and the strong-binding states have been characterized in vitro and in vivo (for review, see Brenner, 1987). Without assuming extra states, but simply by using the rate constants derived from mechanical measurements (Brenner, 1988) and other experimentally observed properties of the weak- and strong-binding states, the crossbridge model of Eisenberg and Hill can describe very well the time course of force and stiffness and of the changes observed in the x-ray diffraction intensities during the rising phase of a tetanus (Brenner, 1989). Therefore, we believe that the structure of the attached crossbridges in the relaxed muscle as determined by our current method samples the attached states before force generation. The rigor state, on the other hand, represents the end state of the ATPase cycle before the crossbridge is recycled to a new start. Any structural change involved in force generation will likely entail a shift from the type of configuration in the low μ relaxed state towards the rigor configuration. Preliminary equatorial x-ray diffraction data from Ca^{++} activated fibers supports the idea that force generation involves a structural change in the attached crossbridges. (Yu and Brenner, 1987).

SUMMARY

In the skinned rabbit psoas muscle, over one-half of the crossbridges are attached to the thin filament in the relaxed state at low ionic strength and low temperature. Analysis of the mass distributions indicates that in the relaxed muscle, the attached myosin heads remain basically distributed around the thick filament backbone, and the domain of the myosin head concentrated around the thin filament is small. Therefore, the overall distribution of mass is not significantly shifted upon attachment. On the other hand, in the rigor configuration, mass distribution of the crossbridges is shifted away from the thick filament backbone, and a larger domain of the myosin head is concentrated around the thin filament. Any structural changes involved in force generation probably entail a shift from the type of configuration of the crossbridge in the attached relaxed state towards the configuration in the rigor state.

APPENDIX

Direct interpretations of density maps derived from five equatorial reflections are hampered by the artifacts created by termination of the Fourier series. To minimize complications brought by series termination, modeling was pursued to produce mass distributions that give intensities consistent with experimental data. Parameters of the models simulating different states were chosen such that the difference maps were also consistent with the experimental data.

The features of the models have been described in the accompanying paper (Yu, 1989). In the unit cell the basic structure consists of a thick filament backbone, annular distribution of myosin heads, a thin filament, and annular distribution of attached crossbridges. Several types of functions were used to describe these mass distributions: (*a*) Gaussian functions for all distributions; (*b*) Gaussian functions for the backbone of the thick filament and the thin filament, but the distributions for the

TABLE 4 Sample parameters for calculating equatorial intensities based on Gaussian models*

Simulated state	σ_M	σ_A	σ_H	σ_B	A_M	A_A	A_H	A_B	R_H	R_B	Ratio	Calculated intensities normalized w.r.t. I_{10}				Experimental intensities normalized w.r.t. I_{10}			
												I_{11}	I_{20}	I_{21}	I_{30}	I_{11}	I_{20}	I_{21}	I_{30}
Relaxed, μ = 20 mM	4.35	3.25	3.0	0.75	52	16	54	8	13.5	4.0	1.5	2.13	0.08	0.03	0.13	1.83	0.11	0.03	0.14
Relaxed, μ = 100 mM	4.50	3.25	3.0	0.75	52	16	58	4	13.5	4.0	1.5	1.09	0.06	0.03	0.07	1.10	0.08	0.03	0.09
Rigor, μ = 100 mM	4.50	3.25	3.0	1.50	52	16	45	12.5	14.0	4.75	1.5	4.77	0.09	0.08	0.12	3.80	0.17	0.08	0.16

*Gaussian functions were used to describe the thick filament backbone (M), the thin filament (A), the annular distribution of myosin heads (H) and the attached crossbridges (B) (Yu, 1989). 4σ is defined as the width and A is the total mass of each structure (M, A, H, B). R_H and R_B are the radial distances of annular distributions H and B from the centers of the thick and the thin filaments, respectively.

myosin heads and the attached crossbridges are flat functions; (*c*) flat functions with cosine shaped edges for all distributions. Qualitative conclusions were found to be insensitive to which type of function was used.

In selecting models, the mass ratio of the backbone of the thick filament and the thin filament was chosen to be in agreement with biochemical data; the resulting density maps after applying radial filter at [3, 0] resemble the experimental data with the phase set (+ + − + +), and more importantly, the difference maps must produce features similar to Figs. 5 and 7.

Parameters for the type *a* Gaussian functions that result in good agreement with experimental intensity data for the relaxed state at μ = 20 and 100 mM and the rigor state at μ = 100 mM are given in Table 4.

Several highlights of the modeling results are the following: for the relaxed state, the widths of the functions describing the attached crossbridges must be small. R_B stays below 4–5 nm from the center of the thin filament. Both radial parameters, R_H and R_B, are required to remain unchanged in the rel→rel case. The rel→rigor case (Fig. 5 *b*) is simulated if σ_B and/or R_B are increased. The increase of density at the center of the thick filament backbone (Fig. 5 *a*) requires a smaller σ_M for the relaxed state at μ = 20 mM compared with that at μ = 100 mM.

We are grateful to Dr. Richard Podolsky of the National Institutes of Health (NIH) for his generosity and for his constant encouragement throughout this work. We thank Drs. Alasdair Steven and Benes Trus of NIH for their help with the PIC image analysis system and for many stimulating discussions. We also gratefully acknowledge many helpful discussions with Drs. J. M. Squire and J. J. Harford of Imperial College, London.

This work is supported in part by a Deutsche Forschungsgemeinschaft grant (Br 849/1-2).

Received for publication 9 December 1987 and in final form 29 August 1988.

REFERENCES

Brenner, B. 1983. Technique for stabilizing the striation pattern in maximally calcium-activated skinned psoas fibers. *Biophys. J.* 41:99–102.

Brenner, B. 1987. Mechanical and structural approaches to correlation of cross-bridge action in muscle with actomyosin ATPase in solution. *Annu. Rev. Physiol.* 49:655–672.

Brenner, B. 1988. Effect of Ca^{2+} on crossbridge turnover kinetics in skinned single rabbit psoas fibers: implications for regulation of muscle contraction. *Proc. Natl. Acad. Sci. USA.* 85:3265–3269.

Brenner, B. 1989. Muscle mechanics and biochemical kinetics. *In* Molecular Mechanisms in Muscular Contraction. J. M. Squire, editor. Macmillan Press Ltd. In press.

Brenner, B., M. Schoenberg, J. M. Chalovich, L. E. Greene, and E. Eisenberg. 1982. Evidence for cross-bridge attachment in relaxed muscle at low ionic strength. *Proc. Natl. Acad. Sci. USA.* 79:7288–7291.

Brenner, B., J. M. Chalovich, L. E. Greene, E. Eisenberg, and M. Shoenberg. 1986. Stiffness of skinned rabbit psoas fibers in MgATP and $MgPP_i$ solution. *Biophys. J.* 50:685–691.

Brenner, B., L. C. Yu, and R. J. Podolsky. 1984. X-ray diffraction evidence for cross-bridge formation in relaxed muscle fibers at various ionic strengths. *Biophys. J.* 46:299–306.

Brenner, B., L. C. Yu, and L. E. Greene, E. Eisenberg, and M. Schoenberg. 1986. Ca^{2+}-sensitive cross-bridge dissociation in the presence of magnesium pyrophosphate in skinned rabbit psoas fibers. *Biophys. J.* 50:1101–1108.

Craig, R., L. E. Greene, and E. Eisenberg. 1985. Structure of the actin-myosin complex in the presence of ATP. *Proc. Natl. Acad. Sci. USA.* 82:3247–3251.

Egelman, E. H., and R. Padron. 1984. X-ray evidence that F-actin is a 100 Å filament. *Nature (Lond.).* 307:56–58.

Eisenberg, E., and T. L. Hill. 1985. Muscular contraction and free energy transduction in biological systems. *Science (Wash. DC).* 227:999–1006.

Fraser, R. D. B., and T. P. MacRae. 1973. Conformations in Fibrous Proteins. Academic Press, Inc., New York. 33.

Goody, R. S., and K. C. Holmes. 1983. Crossbridges and the mechanism of muscle contraction. *Biochim. Biophys. Acta* 726:13–39.

Haselgrove, J. C. 1980. A model of myosin crossbridge structure consistent with the low angle X-ray diffraction pattern of vertebrate muscle. *J. Muscle Res. Cell Motil.* 1:177–191.

Huxley, A. F. 1957. Muscle structure and theory of contraction. *Prog. Biophys. Biophys. Chem.* 7:255–318.

Huxley, H. E. 1968. Structural differences between resting and rigor muscle. Evidence from intensity changes in the low-angle equatorial X-ray diagram. *J. Mol. Biol.* 37:507–520.

Huxley, H. E., and M. Kress. 1985. Crossbridge behavior during muscle contraction. *J. Muscle Res. Cell Motil.* 6:153–161.

Knott, G. 1979. MLAB: A mathematical modeling tool. *Comput. Programs Biomed.* 10:271–280.

Matsuda, T., and R. J. Podolsky. 1984. X-ray evidence for two structural states of the actomyosin cross-bridge in muscle fibers. *Proc. Natl. Acad. Sci. USA.* 81:2364–2368.

Podolsky, R. J., and T. Arata. 1988. Force generation mechanisms in striated muscle. in *Molecular mechanism of muscle contraction.* H. Sugi and G. H. Pollack, editors. Plenum Publishing Corp., New York. 319–330.

Poulsen, F. R., and J. Lowy. 1983. Small-angle X-ray scattering from myosin heads in relaxed and rigor frog skeletal muscles. *Nature (Lond.).* 303:146–152.

Schoenberg, M. 1988. Characterization of the myosin adenosine triphosphate (M·ATP) crossbridge in rabbit and frog skeletal muscle fibers. *Biophys. J.* 54:135–148.

Squire, J. 1981. Structural Basis of Muscular Contraction. Plenum Publishing Corp., New York.

Stewart, M., and R. W. Kensler. 1986. Arrangement of myosin heads in relaxed thick filaments from frog skeletal muscle. *J. Mol. Biol.* 192:831–851.

Trus, B. L., and A. C. Steven. 1981. Digital image processing of electron micrographs—the PIC system. *Ultramicroscopy.* 6:383–386.

Wagner, P. D., and E. Giniger. 1981. Calcium-sensitive binding of heavy meromyosin to regulated actin in the presence of ATP. *J. Biol. Chem. 256:12647–12650.*

Winklemann, D. A., H. Mekee, and I. Rayment. 1985. Packing analysis of crystalline myosin subfragment-1. Implication for the size and shape of the myosin head. *J. Mol. Biol.* 181:487–501.

Wray, J. 1987. Structure of relaxed myosin filaments in relation to nucleotide state in vertebrate skeletal muscle. *J. Muscle Res. Cell Motil.* 8:62.

Xu, S., M. Kress, and H. Huxley. 1987. X-ray diffraction studies of the structural state of crossbridge in skinned frog sartorius muscle at low ionic strength. *J. Muscle Res. Cell Motil.* 8:39–54.

Yu, L. C. 1987. Effects of limited resolution on density maps reconstructed from equatorial X-ray diffraction intensities of skeletal muscle. *Biophys. J.* 51 2, Pt. 2:473a. (Abstr.)

Yu, L. C., and B. Brenner. 1986. High resolution equatorial X-ray diffraction from single skinned rabbit psoas fibers. *Biophys. J.* 49:133–135.

Yu, L. C., and B . Brenner. 1987. Equatorial X-ray diffraction from fully Ca^{++}-activated single muscle fibers at low ionic strengths. *Biophys. J.* 51 2, Pt. 2:473a (Abstr.)

Yu, L. C., A. C. Steven, G. R. S. Naylor, R. C. Gamble, and R. J. Podolsky. 1985. Distribution of mass in relaxed frog skeletal muscle and its redistribution upon activation. *Biophys. J.* 47:311–321.

Yu, L. C. 1989. Analysis of equatorial x-ray diffraction patterns from skeletal muscle. *Biophys. J.* 55:433–440.